Hydrophobic interaction between contiguous residues in the S6 transmembrane segment acts as a stimuli integration node in the BK channel

Willy Carrasquel-Ursulaez,[1,2]* Gustavo F. Contreras,[1]* Romina V. Sepúlveda,[3,4] Daniel Aguayo,[3] Fernando González-Nilo,[1,3] Carlos González,[1] and Ramón Latorre[1]

[1]Centro Interdisciplinario de Neurociencia de Valparaíso and [2]Doctorado en Ciencias Mención Neurociencia, Facultad de Ciencias, Universidad de Valparaíso, Valparaíso 2366103, Chile

[3]Centro de Bioinformática y Biología Integrativa and [4]Doctorado en Biotecnología, Facultad de Ciencias Biológicas, Universidad Andres Bello, Santiago 8370146, Chile

Large-conductance Ca^{2+}- and voltage-activated K^+ channel (BK) open probability is enhanced by depolarization, increasing Ca^{2+} concentration, or both. These stimuli activate modular voltage and Ca^{2+} sensors that are allosterically coupled to channel gating. Here, we report a point mutation of a phenylalanine (F380A) in the S6 transmembrane helix that, in the absence of internal Ca^{2+}, profoundly hinders channel opening while showing only minor effects on the voltage sensor active–resting equilibrium. Interpretation of these results using an allosteric model suggests that the F380A mutation greatly increases the free energy difference between open and closed states and uncouples Ca^{2+} binding from voltage sensor activation and voltage sensor activation from channel opening. However, the presence of a bulky and more hydrophobic amino acid in the F380 position (F380W) increases the intrinsic open–closed equilibrium, weakening the coupling between both sensors with the pore domain. Based on these functional experiments and molecular dynamics simulations, we propose that F380 interacts with another S6 hydrophobic residue (L377) in contiguous subunits. This pair forms a hydrophobic ring important in determining the open–closed equilibrium and, like an integration node, participates in the communication between sensors and between the sensors and pore. Moreover, because of its effects on open probabilities, the F380A mutant can be used for detailed voltage sensor experiments in the presence of permeant cations.

The Journal of General Physiology

INTRODUCTION

Large-conductance Ca^{2+}- and voltage-activated K^+ channels (BK, Slo1) increase their open probability in the presence of membrane depolarization and/or during an increase in the intracellular Ca^{2+} concentration (Marty, 1981; Pallotta et al., 1981; Latorre et al., 1982). The BK channel is one of the most broadly expressed channels in mammals and plays important roles in both excitable and nonexcitable cells. For example, in vascular smooth muscle cells it regulates the contractile tone, in neurons it colocalizes with voltage-dependent calcium channels and is involved in the control of neurosecretion, and in hair cells it is involved in frequency tuning (Lancaster and Nicoll, 1987; Brayden and Nelson, 1992; Gola and Crest, 1993; Edgerton and Reinhart, 2003; Gessner et al., 2005; Miranda-Rottmann et al., 2010). BK channels are tetramers in which the pore-forming α subunit is coded by a single gene (*Slo1*; *KCNMA1*) ubiquitously expressed across mammalian tissues (Toro et al., 1998). However, BK channels display a variety of phenotypes in different cells and tissues as a result of alternative splicing, metabolic regulation and modulation by β (Orio et al., 2002) and γ (Yan and Aldrich, 2012) subunits. This diversity of phenotypes is fundamental for their adequate function in each tissue.

The voltage-sensing domain (VSD) and pore-gating domain (PGD) of BK channels share similarity with voltage-dependent K^+ channels (Kv). However, an evolutionary relationship between them seems distant (Yu and Catterall, 2004). Evidence suggests that pore domains in both channels are different. For instance, the inner pore in BK channels is larger (Brelidze et al., 2003; Li and Aldrich, 2004; Zhou et al., 2011) than in Kv channels. Also, the ion permeation gate of BK channels resides at the selectivity filter (Piskorowski and Aldrich, 2006), whereas that of Kv channels is controlled by an intracellular gate (Liu et al., 1997). Moreover, Zhou et al. (2011) found that BK S6 transmembrane helix residues are rotated relative to Shaker, which is a Kv channel.

*W. Carrasquel-Ursulaez and G.F. Contreras contributed equally to this paper.

Correspondence to Ramón Latorre: ramon.latorre@uv.cl; or Carlos González: carlos.gonzalezl@uv.cl

Abbreviations used in this paper: HA, Horrigan and Aldrich; IbTx, iberiotoxin; MD, molecular dynamics.

© 2015 Carrasquel-Ursulaez et al. This article is distributed under the terms of an Attribution–Noncommercial–Share Alike–No Mirror Sites license for the first six months after the publication date (see http://www.rupress.org/terms). After six months it is available under a Creative Commons License (Attribution–Noncommercial–Share Alike 3.0 Unported license, as described at http://creativecommons.org/licenses/by-nc-sa/3.0/).

The Rockefeller University Press $30.00
J. Gen. Physiol. Vol. 145 No. 1 61–74
www.jgp.org/cgi/doi/10.1085/jgp.201411194

Mutations in the S6 affect BK channel gating. For example, mutations on human BK F380 residue (Lippiat et al., 2000) or its corresponding murine BK-F315 (Wang and Brenner, 2006) have profound effects on gating and unitary conductance. There is evidence that this residue participates in a state-dependent interaction with L312 (L377 in human BK) of a neighboring subunit to hold the channel in the closed configuration (Wu et al., 2009), whereas the neighboring residue M314 (M377 in hSlo) changes its degree of pore exposure during opening (Chen and Aldrich, 2011). Interestingly, Wu et al. (2009) found that mBK F315 mutants show changes in Ca^{2+} and voltage sensitivity, suggesting that this residue participates in the allosteric communication between voltage sensors and the pore gate domain. However, it is difficult to decide which parameters are being affected by the mutations on the basis of macroscopic currents alone. In particular, the mBK mutant (F315A) is able to reach the membrane, but the very small currents detected suggest that either function or expression is impaired in the mutant channel (Wu et al., 2009). Here, we found that the corresponding human mutation (hSlo-F380A), given the large gating currents we detected, is robustly expressed in the oocyte plasma membrane, indicating that expression and voltage sensor movements were not greatly affected. However, ionic currents noticeably changed. In the presence of 100 µM internal Ca^{2+}, a large rightward shift of the voltage activation curve was observed, with a reduction in the apparent voltage sensitivity. In the absence of Ca^{2+}, small ionic currents of BK F380A were detected only at voltages >300 mV. Therefore, F380A mutant gating currents can be observed in solutions containing 110 mM K^+ without interference of ionic currents in a broad range of voltages. Based on the Horrigan and Aldrich (HA) allosteric model for BK channel gating (Horrigan and Aldrich, 2002), these results can be explained by a large increase in the free energy difference between open and closed states and a decrease of the allosteric factors that couple the Ca^{2+} binding with the voltage sensor and the voltage sensor with the pore opening. The same behavior was observed when the 380 residue was mutated to other small hydrophobic amino acids. The behavior of BK F380A makes it an excellent candidate for further understanding BK voltage-dependent activation as gating currents can be measured in the presence of K^+. To test the effects of increasing the hydrophobicity of the 380 residue, we studied the effects of the F380W mutation on BK channel gating. The open–closed equilibrium was increased and the coupling between Ca^{2+} and voltage sensors with the pore domain was severely weakened in the F380W mutant. Our results indicate that the 380 residue participates in a hydrophobic interaction with L377 that stabilizes the open state while functioning as a link for the communication between Ca^{2+} and voltage sensors and the pore domain.

MATERIALS AND METHODS

Site-directed mutagenesis and channel expression

Human BK α subunit (GenBank accession no. U11058) was provided by L. Toro (University of California, Los Angeles, Los Angeles, CA). Full-length cDNA for hSlo1 was subcloned into pBSTA. Mutations were obtained by the QuikChange site-directed mutagenesis kit (Agilent Technologies). The constructs were checked by sequencing. To prepare mRNA, the plasmids were linearized with Enzyme NotI and then in vitro transcribed by mMESSAGE mMACHINE (Ambion). *Xenopus laevis* oocytes were injected with ∼50 ng of α subunit mRNA 4–8 d before recording.

Electrophysiology

Using the patch-clamp technique, ionic currents (I_K) were recorded in inside-out and outside-out configurations, and gating currents (I_g) were recorded in the inside-out configuration only. All of the internal solutions contained (mM) 110 X-$MeSO_3$ and 10 HEPES. 5 mM EGTA was used as Ca^{2+} chelator for "zero Ca^{2+}" solutions. These solutions contained an estimated 0.8 nM, based on the presence of ∼10 µM contaminant [Ca^{2+}] (Cox et al., 1997). 1 mM HEDTA was used as Ca^{2+} buffer for solutions containing 0.1–3 µM free Ca^{2+}. No Ca^{2+} chelator was used in 100 µM free Ca^{2+} solutions. For 0.1–3 µM free Ca^{2+} solutions, $CaCl_2$ was added to reach the desired [Ca^{2+}] from a stock solution containing X mM $CaCl_2$, and HCl was added until reaching 4 mM [Cl^-]. The external (pipette) solution contained (mM) 110 X-$MeSO_3$, 10 HEPES, and 2 $MgCl_2$. I_K currents and unitary channel recordings were recorded using internal and external K^+ instead of X. I_g currents were recorded using impermeant ions in internal solution X = *N*-methyl-D-glucamine (NMDG) and external X = tetraethylammonium (TEA). pH was adjusted to 7 by adding KOH, NMDG, or TEA-OH according to the X component of each solution. Experiments were performed at room temperature (20–22°C). Free calcium concentrations were calculated using the WinMaxChelator Software and checked with a calcium electrode (Hanna Instruments).

Pipettes of borosilicate capillary glass (Corning 7740; Pyrex) were pulled in a horizontal pipette puller (Sutter Instrument). Pipette resistance was 0.5–1 MΩ after being fire-polished. Data were acquired with an Axopatch 200B (Axon Instruments) amplifier. Both the voltage command and current output were filtered at 20 kHz with 8-pole Bessel low-pass filter (Frequency Devices, Inc.). Current signals were sampled with a 16-bit A/D converter (Digidata 1322A; Axon Instruments) at a sampling rate of 500 kHz. Experiments were performed using Clampex 8 (Axon Instruments) acquisition software. Leak subtraction was performed using a P/4 protocol (Armstrong and Bezanilla, 1974).

Nonstationary noise analysis

To determine the unitary conductance of the channels at 100 and −100 mV, we used a nonstationary fluctuation analysis (Sigworth, 1980; Alvarez et al., 2002). The mean current and variance of isochrones were calculated from 200 current relaxation traces in response to a 100-mV pulse and a −100-mV tail pulse. The unitary current was calculated by fitting the variance versus mean current data to a straight line.

Limiting slope analysis

In the case of the F380A mutant, it was possible to obtain the limiting slope of the $P_O(V)$ curve at 0 internal Ca^{2+}. In this case the number of channels, N, was obtained by dividing the maximum ON gating charge by the charge per channel, which was supposed to be 2.4 e_0 (4 z_Q, see below). Because in the case of the F380A mutant we can measure gating currents and macroscopic ionic currents (I) simultaneously, the probability of opening P_O can be calculated as $P_O = I/iN$, where i is the single-channel current. From the noise analysis we have i at −100 mV (i_{-100mV}); however,

the BK $i(V)$ curve is nonlinear. Because we cannot determine the $I(V)$ relation for the F380A single channel, this nonlinearity was taken into account by multiplying i_{-100mV} by the ratio of the macroscopic conductances obtained at the end of the activation pulse and at the beginning of the tail current for the mutant channel at 100 µM Ca^{2+} (see Fig. 1 B) for the same voltages at which the P_O was calculated in Fig. 3 B.

Data analysis

Data analysis was performed using Clampfit 10 (Axon Instruments) and Excel 2007 (Microsoft). OFF gating currents were integrated between 0 and 400 µs after the OFF voltage step to obtain the OFF net charge movement (Q_{OFF}). To obtain the charge displaced between closed states, Q_c, the first 50 µs of the ON gating currents were fitted to a single exponential function and the area under the curve was integrated, as described in Fig. S1. In all cases, leakage current was subtracted by shifting the current by its mean value during 1 ms before the voltage step. $Q_{OFF}(V)$ and $Q_c(V)$ data were fitted using a Boltzmann function:

$$Q(V) = \frac{Q_{MAX}}{1 + e^{\frac{-z_Q F(V - V_0)}{RT}}}, \quad (1)$$

where Q_{MAX} is the maximum charge, z_Q is the voltage dependency of activation, V_0 is the half-activation voltage of gating current, T is the absolute temperature (typically 295 K), F is Faraday's constant, and R is the universal gas constant. Q_{MAX}, V_0, and z_Q were determined by using the Solver complement of Microsoft Excel to find the minimum of the sum of the squares of the differences between experimental and calculated charges. Instantaneous tail currents were fitted to a Boltzmann function of the form

$$G(V) = \frac{G_{MAX}}{1 + e^{\frac{-z_G F(V - V_h)}{RT}}},$$

where G_{MAX} is the maximum tail current, z_G is the voltage dependency of activation, and V_h is the half-activation voltage of the ionic current. All the analyses that follow were performed using G/G_{MAX} or Q/Q_{MAX} values.

To analyze $G(V)$ and $Q(V)$ curves, a mean V_h and V_0 ($<V_h>$, $<V_0>$) values were obtained at each Ca^{2+} concentration. All of the corresponding $G(V)$ and $Q(V)$ curves were aligned by shifting them along the voltage axis by the mean ΔV_h ($<V_h> - V_h$) or ΔV_0 ($<V_0> - V_0$) to get a mean curve that did not alter the voltage dependence. For each mean curve, the data were binned in 25-mV intervals.

Model fitting

We fit the experimental data using the HA model (Horrigan and Aldrich, 2002). In this model the opening reaction is described by the voltage-dependent equilibrium constant L. J is the equilibrium constant that defines the voltage sensor resting–active equilibrium (J), whereas the Ca^{2+} binding is described by the equilibrium K. The model includes allosteric factors between any pair of modules: C, D, and E for the coupling between calcium sensors and pore opening, the coupling of the voltage sensors and pore opening, and the calcium sensor–voltage sensor allosteric coupling, respectively (see Scheme 1 below).

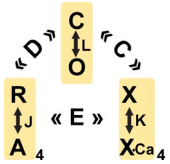

(Scheme 1)

The open probability at any given voltage and Ca^{2+} concentration can be calculated as

$$P_O = \frac{L(1 + JD + KC + JKCDE)^4}{L(1 + JD + KC + JKCDE)^4 + (1 + J + K + JKE)^4},$$

where

$$J = J_0 e^{\frac{z_J FV}{RT}},$$

$$K = \frac{Ca^{2+}}{k_d},$$

and

$$L = L_0 e^{\frac{z_L FV}{RT}}.$$

J_0 is the resting–active equilibrium for the voltage sensor at 0 mV with no calcium bound. L_0 is the equilibrium constant for channel opening with all voltage sensors in the resting state and not calcium bound at 0 mV. The parameter k_d is the dissociation constant of a single calcium-binding site with all voltage sensors at rest and the channel closed. The parameters z_L and z_J are the voltage dependence of the equilibria L and J, respectively.

For WT BK channel, L_0 and z_L were obtained from Orio and Latorre (2005). The equilibrium constant that defines the voltage sensor active–resting equilibrium at zero voltage, J_0, and the apparent number of gating charges per voltage sensor, z_Q, in the absence of Ca^{2+} were obtained from the data shown in Fig. 3 E because

$$Q(V) = \frac{Q_{max} * J}{1 + J},$$

where

$$J = J_0 e^{\frac{z_J FV}{RT}} = e^{\frac{z_Q F(V - V_0)}{RT}}$$

and V_0 is the half-activation voltage of the $Q_c(V)$ curve. Next, we calculated the allosteric parameter E assuming that the fast ON gating currents, Q_c, in the presence of saturating calcium occurs essentially between closed states; in this case J is multiplied by E. So, E can be calculated using the equation

$$JE = J_0 e^{\frac{RT \ln E + z_Q FV}{RT}} = e^{\frac{z_Q^* F(V - V_0^*)}{RT}},$$

where z_Q^* and V_0^* are the voltage dependence and the half-activation voltage of the $Q_c(V)$ curve at 100 µM Ca^{2+}. The values obtained for L_0, z_L, J_0, z_Q, and E were introduced into the model as fixed parameters, and we calculated the allosteric parameter D by minimizing the sum of square of $G(V)$ data in the absence of internal Ca^{2+} with the Solver tool of Excel. Once D was obtained, we performed a global fit to the $G(V)$ data obtained at seven different Ca^{2+} concentrations to estimate C and k_d.

To fit the F380A data, we fixed z_L from Orio and Latorre (2005). E, J_0, and z_Q were calculated using the data for the mutant channel shown in Fig. 3 E in the same manner as we did for the WT channel. k_d was assumed to be identical to WT. Finally, to obtain to L_0, D, and C, the $G(V)$ data obtained at different Ca^{2+} concentrations was globally fitted to the HA model. L_0 and D were fitted without any restriction, except the condition that $L_0 D^4 = 6.59 \times 10^{-5}$ (see Fig. 2 B).

The F380W data were fitted to the HA model using the same z_L as before, and J_0 and z_Q were obtained from the fit to the $Q_r(V)$ data shown in Fig. 4 C in a similar way as was done for WT BK. k_{cl} was supposed as identical to WT. Previous parameters obtained were introduced into the model, and we calculated the allosteric parameters L_0 and D by minimizing sum of the square of $G(V)$ data, in the absence of internal Ca^{2+}. Finally, E and C were obtained by performing a global fit to the $G(V)$ data obtained at different Ca^{2+} concentrations using the HA model.

To test whether a fit parameter was statistically different between two datasets, a global fit in which the parameter of interest was restricted to be equal among all datasets was compared against an independent fit of each dataset. A comparison between independent and global fits was done by an extra sum of squares F test, using the formula

$$F = \frac{\left(SS_{glb} - SS_{ind}\right) / \left(DF_{glb} - DF_{ind}\right)}{SS_{ind} \,/\, DF_{ind}},$$

where SS and DF are the sum of squares and the degrees of freedom of the fit, respectively; glb and ind denote the global and the independent fit, respectively. All of the analyses were performed with Excel, and the conversion of the F values to p-values was performed with Prism software (GraphPad Software). P-values <0.01 were considered significant.

Molecular modeling

BK 3-D model was built using the sequence of human BK channel (UniProt ID: Q12791) stored in GenPept. Based on the sequence alignment of Carvacho et al (2008), the segments S5–S6 were aligned against the sequence of MthK crystal in Protein Data Bank (accession no. 4HYO; Posson et al., 2013), achieving 35% of sequence identity. Several models were obtained using Modeller v9.10 (Sali and Blundell, 1994), from which the lowest energy structure based on DOPE potential was chosen to build a tetrameric model by structural aligning with MthK crystal structure. The resulting model was then evaluated using the ANOLEA software (Melo and Feytmans, 1998).

The BK pore structure was embedded on a lipid membrane of phosphatidyl oleoyl phosphatidylcholine (POPC) hydrated with TIP3P water and neutralized by means of counterions at 0.110 M KCl. Also, potassium ions were located on sites S0, S2, and S4 of the selectivity filter as used by Moscoso et al. (2012). The final dimensions of the system were ∼12.5 × 12.5 × 12.0 nm^3 and it was constituted by ∼370,000 atoms. Next, the system was submitted to a molecular dynamics (MD) protocol. In brief, a first stage of 2,000 steps of energy minimization and 10 ns of equilibration was performed using an NPT ensemble at 298 K and 1 atm. Also, harmonic restraints of 0.5 kcal/mol*$Å^2$ on C-α were applied to preserve the secondary structure of the model. F380A and F380W BK mutant systems were generated from the equilibrated BK WT system using the VMD mutator plugin (Humphrey et al., 1996). After equilibration, several production simulations were performed for each system, which altogether lasted ∼40 ns. On the production phase, harmonic restraints of 0.2 kcal/mol*$Å^2$ were defined for C-α of segment S5, allowing freedom of segment S6 for further analysis.

All MD simulations were performed with the software NAMD 2.9 (Phillips et al., 2005) using the CHARMM27 (Patel et al., 2004) and CHARMM36 (Klauda et al., 2010) force fields. Bonded and short- and long-range nonbonded interactions were integrated with a time step of 2, 2, and 4 fs, respectively. An 8-Å spherical cutoff was used for short-range nonbonded interactions, including a switching function from 7 Å for the van der Waals term and shifted electrostatics (Wells et al., 2012). The particle-mesh Ewald (PME) method was used with a grid spacing of ∼1 Å.

Online supplemental material

This supplemental material contains one figure and its legend. Fig. S1 shows two examples of the way we determined the fast component of the ON gating current. Online supplemental material is available at http://www.jgp.org/cgi/content/full/jgp.201411194/DC1.

RESULTS

Mutations in the F380 residue produce large changes in conductance-voltage relationships

Macroscopic ionic currents for WT BK and the F380 mutants F380A and F380W in the nominal absence of internal Ca^{2+} and in the presence of several different Ca^{2+} concentrations were characterized in inside-out patches. Representative current records at nominally 0 and 100 µM internal Ca^{2+} concentrations are shown in Fig. 1 (A–C). At 100 µM internal Ca^{2+}, the two BK high-affinity Ca^{2+}-binding sites were saturated, whereas at 0.8 nM (nominal "0" Ca^{2+}) the Ca^{2+}-binding sites were empty (Cox et al., 1997). Fig. 1 B shows that robust F380A currents can be recorded in the presence of several internal Ca^{2+} concentrations, but their behavior is quite different from the currents induced by the WT BK channel (Fig. 1 A). The faster kinetics and the lack of inward currents elicited by the test pulse both indicate that the voltages required to open the mutant channel are much larger compared with those required to activate WT BK channels. In fact, Fig. 1 E shows that although internal Ca^{2+} is able to promote a leftward shift in the F380A voltage-activation curve ($G(V)$), considerably larger voltages compared with the WT BK channel are needed to activate the F380A mutant channel (Fig. 1 D). This mutation also produces a significant decrease in apparent voltage dependence compared with the WT BK (Fig. 1, compare D and E). In the absence of intracellular calcium, the mutant F380A $G(V)$ could not be measured, probably because it is right-shifted to positive voltages that were too large to be experimentally unreachable.

To understand the effects of substituting F380 with other hydrophobic amino acids, we tested mutants F380W, F380L, and F380I. Interestingly, introducing a larger and more hydrophobic amino acid in position 380 (F380W) produces a leftward shift of the $G(V)$ in the absence of Ca^{2+} and at saturating Ca^{2+} concentrations (Fig. 1, C and F) compared with the WT BK. Surprisingly, at the two higher internal Ca^{2+} concentrations tested, a large fraction of channels remained open even at voltages so negative as −200 mV. In contrast, we found that at 100 µM Ca^{2+}, the gating of mutants F380L and F380I was very similar to that of F380A (Figs. 1, G–I).

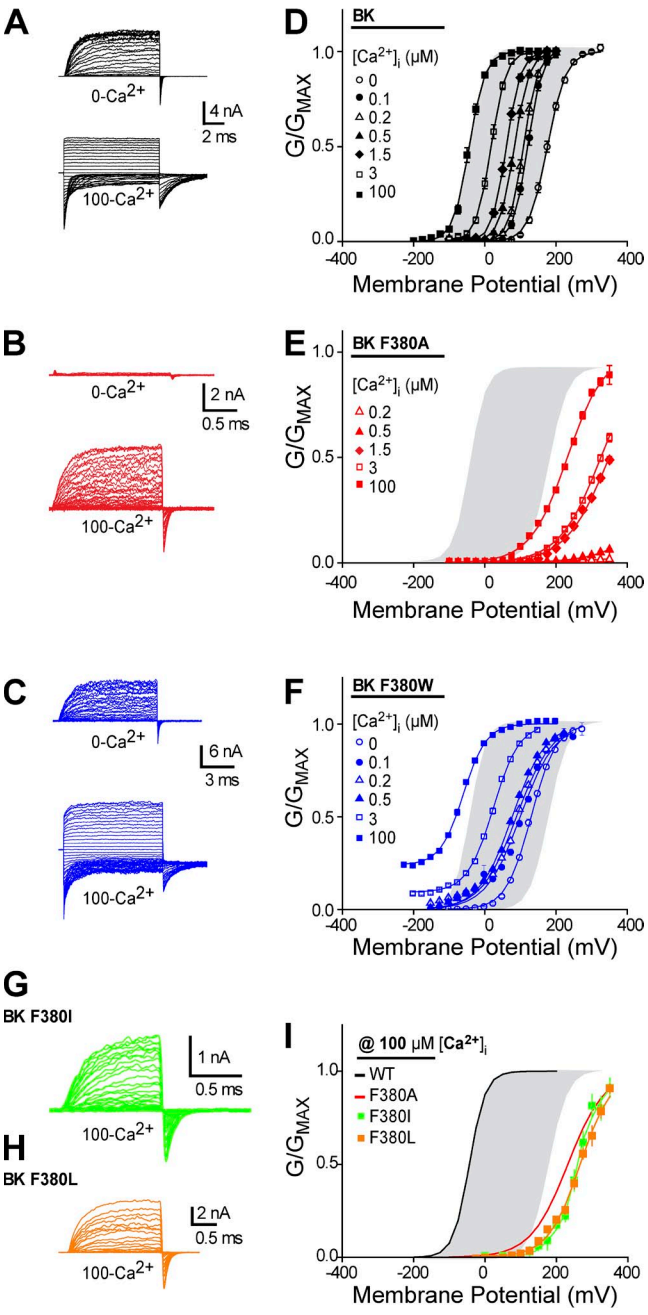

Figure 1. Characterization of BK F380 mutant ionic currents. (A) BK-WT currents (I_K) evoked by voltage steps (−100 to 300 mV; in 10-mV steps of 10 ms) at two different $[Ca^{2+}]_i$ (0 and 100 μM). (B) BK-F380A macroscopic currents recorded at 0 and 100 μM (−100 to 350 mV; in 10-mV steps of 2 ms). Note the difference in time scale because of the fast activation in the case of BK-F380A. (C) BK-F380W currents (I_K) evoked by voltage steps (−220 to 300 mV; in 10-mV steps of 10 ms) in two different $[Ca^{2+}]_i$ (0 and 100 μM). (D–F) Relative conductance versus voltage ($(G/G_{MAX}) - V$) curves were obtained from tail current measurements from experiments as those shown in A–C. Data were fitted using a Boltzmann function (solid lines). For the BK-WT channel, parameters were (mean ± SEM) $V_h = 176 \pm 8$ mV, $z_G = 0.96 \pm 0.08$ e_0 at $[Ca^{+2}]_i = 0$ μM, $n = 5$; $V_h = 120 \pm 10$ mV, $z_G = 1.30 \pm 0.10$ e_0 at $[Ca^{+2}]_i = 0.1$ μM, $n = 5$; $V_h = 110 \pm 8$ mV, $z_G = 1.40 \pm 0.10$ e_0 at $[Ca^{+2}]_i = 0.2$ μM, $n = 6$; $V_h = 81 \pm 5$ mV, $z_G = 1.33 \pm 0.12$ e_0 at $[Ca^{+2}]_i = 0.5$ μM, $n = 5$; $V_h = 52 \pm 8$ mV, $z_G = 1.40 \pm 0.06$ e_0 at $[Ca^{+2}]_i = 1.5$ μM, $n = 5$; $V_h = 20 \pm 6$ mV, $z_G = 1.34 \pm 0.11$ e_0 at $[Ca^{+2}]_i = 3$ μM, $n = 6$; $V_h = -43.7 \pm 11$ mV, $z_G = 1.12 \pm 0.04$ e_0 at $[Ca^{+2}]_i = 100$ μM, $n = 5$. BK-F380A: $V_h = 620 \pm 34$ mV, $z_G = 0.32 \pm 0.03$ e_0 at $[Ca^{+2}]_i = 0.2$ μM, $n = 4$; $V_h = 492 \pm 19$ mV, $z_G = 0.43 \pm 0.02$ e_0 at $[Ca^{+2}]_i = 0.5$ μM, $n = 4$; $V_h = 349.8 \pm 11.7$ mV, $z_G = 0.42 \pm 0.01$ e_0 at $[Ca^{+2}]_i = 1.5$ μM, $n = 5$; $V_h = 321 \pm 9$ mV, $z_G = 0.45 \pm 0.01$ e_0 at $[Ca^{+2}]_i = 3$ μM, $n = 4$; $V_h = 232 \pm 25$ mV, $z_G = 0.48 \pm 0.05$ e_0 at $[Ca^{+2}]_i = 100$ μM, $n = 5$; BK-F380W: $V_h = 133 \pm 3$ mV, $z_G = 0.73 \pm 0.03$ e_0 at $[Ca^{+2}]_i = 0$ μM, $n = 17$; $V_h = 102 \pm 6$ mV, $z_G = 0.52 \pm 0.02$ e_0 at $[Ca^{+2}]_i = 0.1$ μM, $n = 6$; $V_h = 92 \pm 7$ mV, $z_G = 0.52 \pm 0.01$ e_0 at $[Ca^{+2}]_i = 0.2$ μM, $n = 7$; $V_h = 80 \pm 5$ mV, $z_G = 0.55 \pm 0.03$ e_0 at $[Ca^{+2}]_i = 0.5$ μM, $n = 7$; $V_h = 26 \pm 5$ mV, $z_G = 0.70 \pm 0.01$ e_0 at $[Ca^{+2}]_i = 3$ μM, $n = 7$; $V_h = -58 \pm 3$ mV, $z_G = 0.52 \pm 0.03$ e_0 at $[Ca^{+2}]_i = 100$ μM, $n = 14$. (G and H) BK-F380I and BK-F380L currents (I_K) evoked by voltage steps (−100 to 350 mV; in 10-mV steps of 2 ms) at $[Ca^{2+}]_i = 100$ μM, respectively. (I) Relative conductance versus voltage ($(G/G_{MAX}) - V$) curves were obtained from tail current measurements from the experiments shown in G and H. Data were fitted using a Boltzmann function (solid lines). For the BK-F380I channel, parameters were (mean ± SEM) $V_h = 261 \pm 6$ mV, $z_G = 0.72 \pm 0.08$ e_0 at $[Ca^{+2}]_i = 100$ μM, $n = 4$. BK-F380L: $V_h = 267 \pm 6$ mV, $z_G = 0.58 \pm 0.04$ e_0 at $[Ca^{+2}]_i = 100$ μM, $n = 7$. Black and red lines are the $G/G_{MAX} - V$ curves and Boltzmann fitting of the BK channel WT and F380A mutant at $[Ca^{+2}]_i = 100$ μM (as is seen in D and E), respectively.

F380A decreases single-channel conductance and modifies gating kinetics without effects on the voltage dependence of the deactivation kinetics

We tested whether the F380A channel was a bona fide BK channel by analyzing its sensitivity to iberiotoxin (IbTx), known to be a potent and specific blocker of BK channels (Galvez et al., 1990; Candia et al., 1992; Giangiacomo et al., 1992; Kaczorowski and García, 1999). The effect of the toxin was checked in outside-out membrane patches. In the presence of 100 μM internal Ca^{2+}, the current elicited by a 150-mV pulse was measured at different times in the presence of 100 nM IbTx in bath solution (Fig. 2 A). In the presence of the toxin, currents decreased with time and were completely abolished after 5 min (t_3). We also attempted to detect F380A mutant currents in the absence of internal Ca^{2+}. In this case, the test pulse was 350 mV and robust gating currents and relative small ionic currents were observed (Fig. 2 B). These ionic currents were fully blocked by IbTx after 5-min incubation. We concluded that these currents also are mutant BK channels instead of currents induced by oocyte endogenous channels.

Although it is possible to record unitary channels of WT BK and F380W in the absence of internal Ca^{2+}, because of the very fast deactivation kinetics and the very low open probability at the voltages that unitary channels are typically recorded, we were unable to observe individual F380A channel openings (Fig. 2 C). Therefore, we determined unitary conductance by using noise analysis (Sigworth, 1980; Alvarez et al., 2002). Unitary conductance of the mutants F380A and F380W (96 ± 6 pS and 106 ± 3 pS, respectively; mean ± SEM) was reduced compared with that of the WT channel (222 ± 20 pS; Fig. 2, D–F).

A detailed study of the deactivation kinetics in a wide range of voltages indicates that, as expected from the $G(V)$ data, the whole $\tau(V)$ curve for the F380A mutant shifts to the right along the voltage axis (Fig. 2 G). At very negative voltages, only the backward closing rate constants contribute to $\tau(V)$, and the results in Fig. 2 G show that the closing rate of the F380A mutant becomes about fivefold faster with little effect on its voltage dependence compared with that of the WT channel. Note in Fig. 2 G that very fast deactivation kinetics of F380A would produce very brief openings at the single channel level, which could be difficult to record.

Characterization of BK F380A mutant gating currents in the absence and presence of Ca^{2+}

We were able to detect gating currents (I_g) of the F380A mutant in the presence (Fig. 3 A, inset) and absence (Fig. 3 D) of K^+ by using the inside-out patch-clamp configuration. Unlike WT BK, F380A gating currents can be measured in the presence of symmetrical 110 mM K^+ with minimal ionic current contamination (Fig. 3 A, inset). Note that the $Q_c(V)$ curves for F380A in the presence and absence of permeant cations are almost identical (Fig. 3 A).

Unfortunately, as discussed above, it was not possible to observe individual openings of F380A mutant, making it impossible to measure the probability of opening at very negative voltages (limiting slope determination) to obtain a direct estimate of the equilibrium constant that governs the closed–open equilibrium, L. Instead, thanks to the large rightward shift of the $G(V)$ promoted by the F380A mutant, we were able to calculate the limiting slope at voltages at which all voltages sensors are activated (Fig. 3 A). We used recordings as in Fig. 3 A (inset) to calculate the open probability at voltages from 300 mV (Fig. 3 B). To calculate the open probability, we estimated the total number of channels from the quotient between Q_{MAX} in the patch and the charge per channel (estimated to be 4 z_J = 2.4 e_0 from the slope of the $Q_c(V)$). Once obtained, the $P_O(V)$ curve (Fig. 3 B), we can determinate the voltage dependence of the intrinsic open–closed equilibrium, z_L, and the equilibrium constant to 0 mV, L_0*, by using the HA allosteric model, which predicts

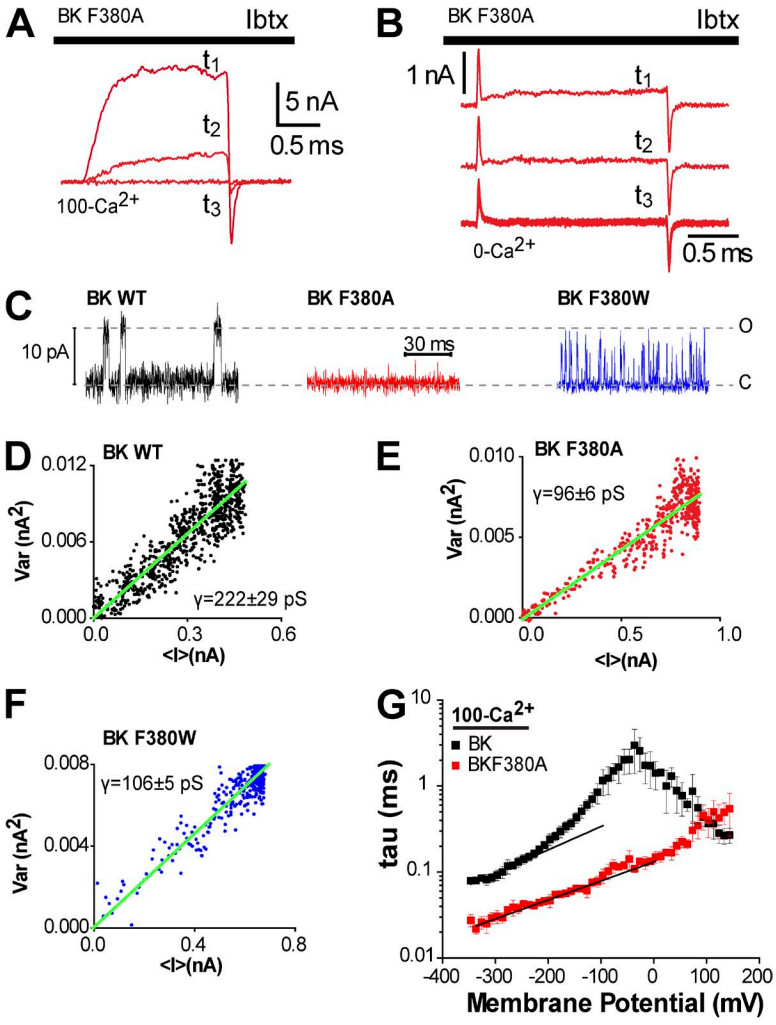

Figure 2. Characterization of BK F380A mutant. (A) IbTx blocks the BK-F380A mutant channel. Currents elicited by a 150-mV pulse were recorded in outside-out patches and symmetrical K^+ 110 mM. The bath solution contained 100 nM IbTx, $[Ca^{2+}]_i$ = 100 µM. Currents were recorded immediately before (t_1), 1 min after (t_2), and 5 min after IbTx addition (t_3). (B) I_g and leak currents were recorded in symmetrical 110 mM K^+ and internal 0 Ca^{2+}, and the pipette solution contained 500 nM IbTx. Currents were recorded immediately after gigaseal formation (t_1), after 1 min (t_2), and after 5 min (t_3). (C) Single-channel recordings of WT BK, F380A, and F380W in the absence of internal Ca^{2+} and upon depolarization at 50 mV. To elicit F380A mutant current, we used a huge pipette, ~30–40 µm. (D–F) Nonstationary noise analysis of BK-WT, BK-F380A, and BK-F380W. Inside-out patches were held to 0 mV and pulsed 200 times from −100 to 100 mV at steps of 2-ms, 10-ms, and 10-ms duration for F380A, F380W, and WT, respectively. $[Ca^{2+}]_i$ = 100 µM. (G) Voltage dependence of deactivation time constants (mean ± SEM) for the WT and F380A channels. Voltage dependence of deactivation rates were calculated from the slope of the straight lines (solid lines) at very negative potentials: z_γ = 0.159 for WT; z_γ = 0.138 for F380A. Deactivation rates at 0 mV were estimated by extrapolating the straight lines: γ_0 = 1,494/s for WT; γ_0 = 7,243/s for F380A.

that under these experimental conditions the open probability is

$$P_O = LD^4 / \left(1 + LD^4\right). \quad (2)$$

Therefore, $L_0^* = L_0 D^4$ obtained from extrapolation of the $P_O(V)$ data of Fig. 3 B to 0 mV represents the product between the intrinsic equilibrium constant, L_0, and the allosteric factor describing the interaction between channels opening and voltage sensor activation, D, to the fourth power. The value of $L_0 D^4 = 6.6{*}10^{-5}$ and $z_L = 0.42$ obtained from the fitting to the $P_O(V)$ data show in Fig. 2 B to Eq. 2 was used as a further constraint when performing the global fit of the $G(V)$ data of Fig. 6 A using the HA model. The value z_L found using this method agrees reasonably with the value obtained by Orio and Latorre (2005).

Robust gating currents for both WT and mutant channels can be recorded in the absence and presence of 100 µM internal Ca^{2+} (Fig. 3, C and D). In both cases, because of the very fast opening kinetics, to obtain only the gating current displaced between closed states, the gating charge was calculated by adjusting the first 50 µs of the ON gating currents to a single exponential and integrating the area under the curve. Compared with WT BK channels, F380A shifts the gating charge-voltage ($Q_c(V)$) curve along the voltage axis to the left by 20 mV in the absence of calcium with no appreciable changes in the voltage dependency of activation z_Q (Fig. 3 E). The values of the half-activation voltage of gating currents in the absence of internal Ca^{2+}, V_0, and z_Q for the WT channel are in reasonable agreement with those previously reported (Horrigan and Aldrich, 1999, 2002; Bao and Cox, 2005; Contreras et al., 2012). Increasing intracellular Ca^{2+} promotes a leftward shift of the $Q_c(V)$ curve for both the WT BK and the F380A mutant, accompanied by an increase in z_Q. In the presence of 100 µM Ca^{2+}, the half-activation voltage for the WT BK and the F380A mutant were 29 mV and 72 mV, respectively (Fig. 3 E). This result suggests that in the F380A mutant the interaction between voltage sensor activation and calcium binding has been weakened. Our results widely differ from that of Horrigan and Aldrich (2002) because they did not observe as large of changes in the half-activation voltage of the $Q_c(V)$ in the presence of internal 70 µM Ca^{2+}.

We note here that the half-activation voltage for the $G(V)$ and $Q_c(V)$ curves for the WT BK channel in 100 µM internal Ca^{2+} are −44 mV and 29 mV, respectively. These results indicate that when, on average, half of the channels are open, only 14% of the total gating charge has been displaced. Therefore, in the presence of saturating internal Ca^{2+}, opening can proceed from deep closed states. Actually, when almost all BK channels are open, only ∼50% of the total voltage sensors have been activated.

Characterization of BK and F380 mutants gating currents in the absence of Ca^{2+}

To study the effects of other F380 mutations on voltage sensor activation, families of I_g, as those shown in Fig. 4 (A–C, insets), evoked at different voltages (−90 to 350 mV), were determined for the fast ON gating current to

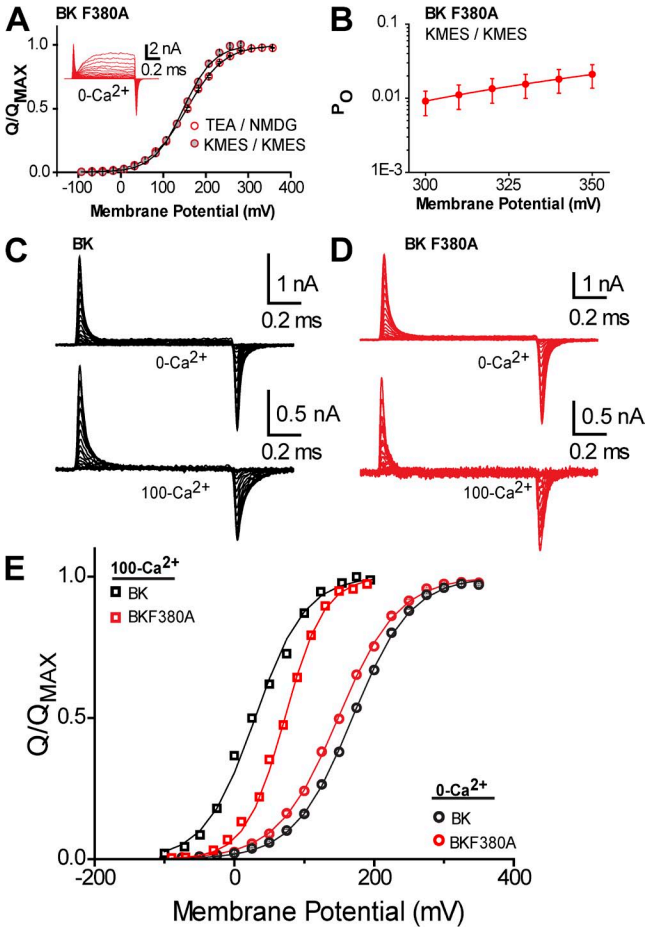

Figure 3. Gating currents of BK-F380A mutant. (A) Fast ON gating charge versus voltage curves obtained in the presence of symmetrical 110 mM KMES (closed circles) and in the absence of permeant ions (open circles), the inset shows the gating and macroscopic currents in the presence of permeant ions (KMES). I_g BK-F380A was recorded in inside-out macropatches at 0 $[Ca^{+2}]_i$ (inset). (B) Open probability versus voltage curve (mean ± SEM) was obtained from F380A mutant current record shown in the inset of A and calculated as was described in Materials and methods. The best fitting of this data to a monoexponential curve was $L^*(V) = L_0^* e^{\frac{z_L FV}{RT}} = L_0 D^4 e^{\frac{z_L FV}{RT}} = 6.59 * 10^{-5} e^{16.5V}$. (C and D) I_g of BK and BK-F380A was recorded from inside-out macropatches at 0 and 100 µM of $[Ca^{+2}]_i$. To isolate I_g of all ionic currents and I_{leak}, our internal and external solutions contained nonpermeant ions (see Materials and methods). I_g was evoked by 2-ms voltage steps of 10 mV, going from −90 to 350 mV. (E) $Q_c(V)$ relationships of BK and BK-F380A were obtained by integrating the fast component for each ON I_g trace. Boltzmann fitting to the experimental data (mean ± SEM) is indicated by solid lines (V_0 = 169 ± 3 mV, z_Q = 0.63 ± 0.02 e_0 in BK at $[Ca^{+2}]_i$ = 0 µM, n = 14; V_0 = 29 ± 8 mV, z_Q = 0.71 ± 0.07 e_0 in BK at $[Ca^{+2}]_i$ = 100 µM, n = 3; V_0 = 149 ± 3 mV, z_Q = 0.59 ± 0.01 e_0 in BK-F380A at $[Ca^{+2}]_i$ = 0 µM, n = 9; V_0 = 72 ± 3 mV, z_Q = 0.87 ± 0.05 e_0 in BK-F380A at $[Ca^{+2}]_i$ = 100 µM, n = 3).

obtain the gating charge activation ($Q_c(V)$) relationships. $Q_c(V)$ data were fitted using Boltzmann functions, normalized to their maxima, and averaged to yield the results shown in Fig. 4 (A–C). Mutations F380I and F380L did not change voltage sensor activation significantly (Fig. 4 D). These results suggest that the F380 mutations to I or L do not affect the voltage sensor conformational changes that accompany the changes in applied membrane voltage but profoundly modify the channel gating uncoupling voltage sensor activation and pore and/or modifying the intrinsic closed–open equilibrium. In contrast, a large hydrophobic amino acid such as tryptophan slightly facilitates opening (Fig. 1, C and F) without greatly affecting the voltage sensor workings (Fig. 4 C). Thus, this suggests that the presence a strong hydrophobic amino acid in position 380 is needed for the adequate functioning of the channel.

F380A diminishes slow gating charge recovery in the absence of intracellular Ca^{2+}

A two-state model (i.e., resting–active) is adequate to describe the early movement of the voltage sensor in the BK (Horrigan and Aldrich, 1999). Late conformational changes of the voltage sensor produce a slow component of the gating charge that can be measured in the OFF gating current. To test the existence of a slow component, we searched for increases in the OFF net gating charge, Q_{OFF}, after voltage pulses of increasing duration were applied, as shown in Fig. 5 A. The origin of this slow component can be explained in terms of an allosteric voltage-gating scheme (Horrigan and Aldrich, 2002). This model predicts that the slow OFF gating charge develops with a time constant that is limited by the speed of channel opening (Horrigan and Aldrich, 1999). The slow component is quite reduced in the mutant compared with WT channel (Fig. 5, B and C). This result suggests that although the opening of WT occurs mainly when three or four voltage sensors are active, necessarily the opening of mutant channel occurs when all voltage sensors are active because of the weak voltage dependency of pore opening. We argue that the slow component is simply a consequence of the number of channels that were open at the end of a long duration voltage pulse (Horrigan and Aldrich, 2002). For example, in the case of the 200-mV pulse, most WT BK channel can reach the open configuration (Fig. 5 D). In this case, the OFF gating charge develops with a time constant close to the time constant that describe the activation of the ionic currents (Fig. 5 B). However, in the case of the F380A channel, the dramatic decrease in the slow component (Fig. 5 C) is simply a reflection of the very low probability of channel opening at 200 mV, and most of the gating charge is displaced between closed states (Fig. 5 E).

F380A mutation affects the closed–open equilibrium and coupling of voltage sensor activation to channel opening

To determine how the F380A and F380W mutations affect the phenotype of the BK channel, we fit our results to the HA allosteric model for WT BK and both mutants (Fig. 6, A–C). First, we fit the data of the WT BK using as initial values for the parameters of the model those reported by Orio and Latorre (2005), but using the z_J and J_0 values calculated from fitting the $Q_c(V)$ curves to a Boltzmann function in the absence of intracellular calcium (Fig. 3 E), the E parameter was calculated as

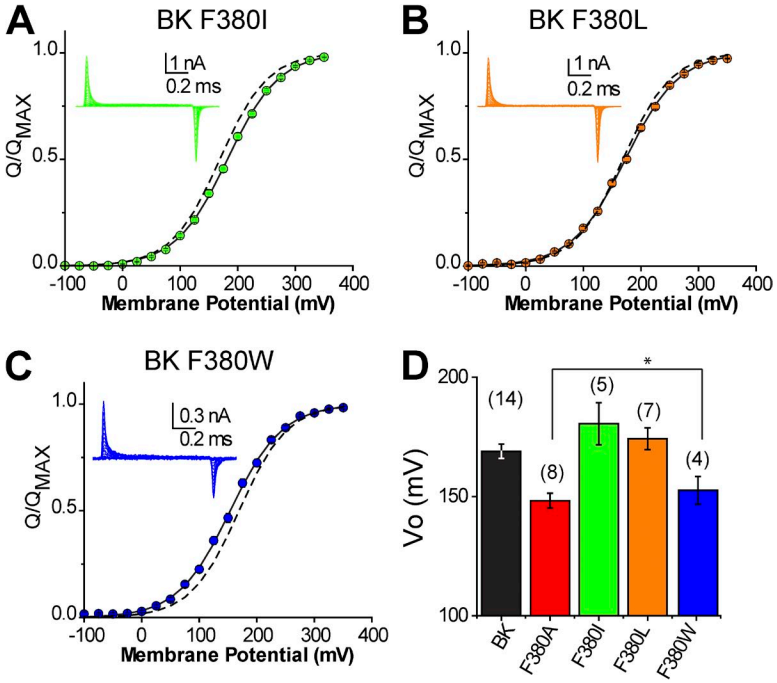

Figure 4. Gating currents of BK-F380 mutants in internal calcium absence. (A–C, insets) I_g of mutants (F380I, F380L, and F380W) was recorded in inside-out macropatches at 0 µM $[Ca^{+2}]_i$. I_g was evoked by 2-ms voltage steps of 10 mV going from −90 to 350 mV. (A–C) $Q_c(V)$ relationships of BK and BK-F380 mutants were obtained by integrating each I_g trace. Boltzmann fitting to the experimental data (mean ± SEM) is indicated by solid lines (V_0 = 182 ± 9 mV, z_Q = 0.56 ± 0.01 e_0 in BK-F380I, n = 5; V_0 = 173 ± 4 mV, z_Q = 0.55 ± 0.01 e_0 in BK-F380L, n = 7; V_0 = 153 ± 6 mV, z_Q = 0.56 ± 0.02 e_0 in BK-F380W, n = 4). Dashed lines represent the Boltzmann fitting to the WT $Q_c(V)$ obtained in the absence of intracellular Ca^{2+} (Fig. 3 E). (D) V_0 of $Q_c(V)$ of mutants (F380I, F380L, and F380W) compared with $Q_c(V)$ of WT and F380A. Mean ± SEM.

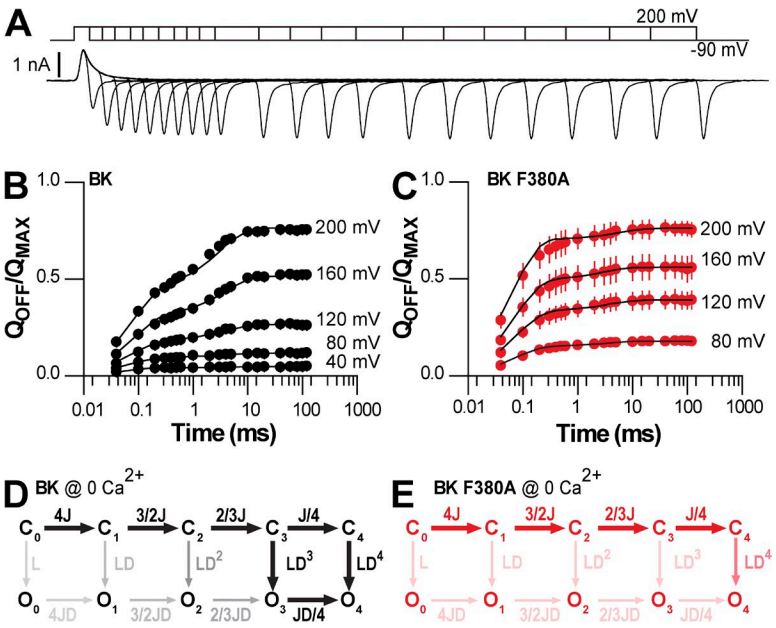

Figure 5. Slow gating charge recovery of WT and F380A. (A) Representative recording of gating currents evoked by 200-mV pulses with different durations from 0.04 to 120 ms. (B and C) Slow gating charge kinetics of BK and BK-F380A. The OFF charge (Q_{OFF}; filled circles; mean ± SEM) was integrated in a range of 1 ms, normalized to the Q_{MAX} for each patch, and plotted against the pulse duration (time; logarithmic scale) for different voltage steps (40, 80, 120, 160, and 200 mV). The $Q_{OFF}/Q_{MAX} - t$ relations were fitted with a two-component exponential function (solid line) with time constant and amplitude of the fast component constrained to the exponential fit of I_{gON} at these voltages. (D and E) 10-state allosteric model proposed for WT and mutant F380A channel, respectively. Darkness of the arrows indicates the probability of transitions.

described in Materials and methods using the results of Fig. 3 E, and z_L and L_0 were obtained from Orio and Latorre (2005). The final values of the different parameters were obtained as described in Materials and methods. The parameters obtained for WT were in good agreement with those previously reported except for C and E, which were smaller and greater, respectively. The E value was surprisingly large compared with those reported in the literature (e.g., Horrigan and Aldrich, 2002; Orio and Latorre, 2005). However, we argue that there are no assumptions in the determination of this parameter because it was directly obtained from the gating charge experimental data.

The parameters of the model obtained for WT plus those obtained from the $Q_g(V)$ curves of F380A mutant were used as starting values to perform a global fit of the $G(V)$ for F380A mutant voltage activation at different Ca^{2+} concentrations data (Fig. 6 B). The fit is reasonably

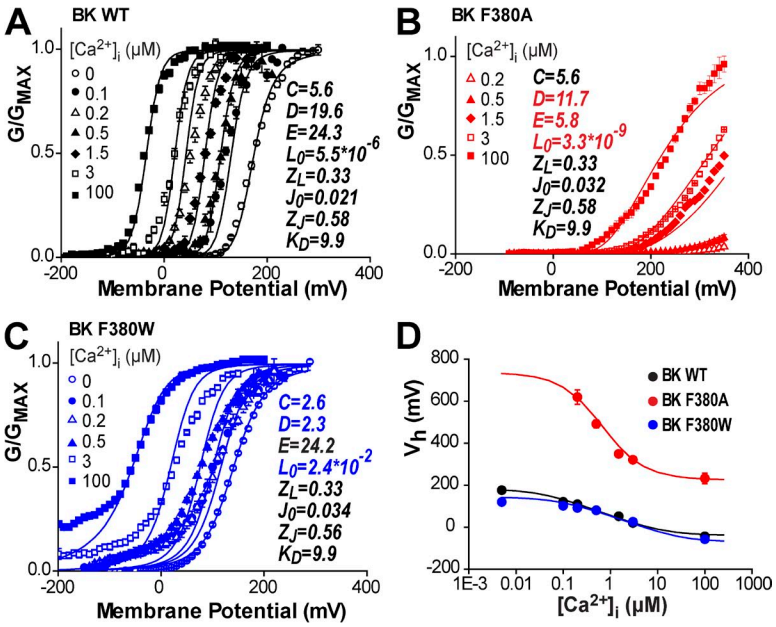

Figure 6. Model fitting. (A) BK WT data (mean ± SEM) were fitted with the HA kinetic model (Horrigan and Aldrich, 2002) as is described in Materials and methods (final parameter values were $L_0 = 5.5 \times 10^{-6}$, $z_L = 0.33$ e_0, $J_0 = 0.021$, $z_J = 0.58$ e_0, $k_d = 9.9$ μM, $C = 5.6$, $D = 19.6$, $E = 24.2$). (B) F380A data (mean ± SEM) were fitted with the HA kinetic model. Effects of mutation on the gating can be explained by a decrease in the allosteric parameter between calcium binding and opening ($C = 5.6$; $P < 0.01$), the allosteric parameter between the voltage sensor activation and opening ($D = 11.7$; $P < 0.01$), the allosteric parameter between the calcium binding and the voltage sensor activation ($E = 5.8$; $P < 0.01$), and a large decrease in the open–closed intrinsic equilibrium constant ($L_0 = 3.3 \times 10^{-9}$; $P < 0.01$). Those parameters whose change was significant are colored in red. (C) F380W data (mean ± SEM) were fitted with the HA kinetic model. Effects of mutation on the gating can be explained by a decrease in the allosteric parameter between calcium binding and opening ($C = 2.6$; $P < 0.01$), the allosteric parameter between the voltage sensor activation and opening ($D = 2.3$; $P < 0.01$), and a large increase in the open–closed intrinsic equilibrium constant ($L_0 = 4.2 \times 10^{-2}$; $P < 0.01$). Those parameters whose change was significant are colored in blue. (D) Experimental V_h (mean ± SEM) of WT BK, F380A, and F380W versus the predicted V_h to different internal Ca^{2+} concentration using the HA allosteric model with the parameters obtained in A–C.

good and indicates that the F380A mutation produces a large increase in the free energy difference between open and closed states and uncouples voltage sensor activation from pore opening and calcium binding from voltage sensor activation. After having all of the parameters that describe the behavior of the F380A mutant, we were able to simulate the $P_O(V)$ curve for the opening of the mutant in the absence of Ca^{2+}. We found that V_h for the F380A mutant under these experimental conditions would be near 737 mV (Fig. 6 D), thus explaining the difficulty of observing ionic currents in the absence of Ca^{2+}.

The parameters obtained for WT plus those obtained from the $Q_c(V)$ curves of F380W mutant (kept fixed) were used as starting values to perform the fit of F380W $G(V)$ at several internal calcium concentrations (Fig. 6 C). Note that F380W produces an increase in L_0 and decrease in D, similar to murine F315Y (Wang and Brenner, 2006), another hydrophobic substitution in the corresponding residue in murine BK. Interestingly, this mutation did not produce significant changes in E but produced a decrease in C (Fig. 6 C). Note that the two higher internal Ca^{2+} concentrations that produce a large fraction of channel remain open at very negative voltages. This behavior is not predicted by the HA model. This phenomenon requires further study, and we will not deal with it further in the present study.

F380 mutant modifies the channel vestibule properties at an atomic scale

We performed an MD simulation of the BK pore region using the open MthK crystal structure as a template. Despite the fact that the inner pore of BK channels appears to be larger than that of MthK (Zhou et al., 2011), we think that the structural model of the BK channel pore depicted in Fig. 7 A represents an open channel because it is able to conduct K^+ ions in silico (not depicted). Fig. 7 A shows the structural model of a WT BK pore embedded in a lipid bilayer after 20 ns of MD simulation. As can be seen in Fig. 7 B, for the WT system, F380 and L377 side chains of the adjacent subunit are tightly locked in the internal vestibule; these residues form a hydrophobic ring (Fig. 7 C). These results are in agreement with the model previously described by Wu et al. (2009). A disruption of the hydrophobic ring formed by 380–377 residues is detected in the F380A channel (Fig. 7 D). The extent of impairment of the interaction between residues located in positions 380 and 377, the nonbonded (van der Waals and coulombic) energy calculated, was ∼20 kJ/mol in the F380A mutant, indicating that the interaction between residues became weaker (Fig. 7 F) compared with the WT BK channel taken as reference. In contrast, our simulations suggest that the interaction between the tryptophan 380 and leucine 377 (Fig. 7 E) is stronger than that between F380 and L377 and amounts to −16.6 kJ/mol (Fig. 7 F).

DISCUSSION

The intracellular mouth of Kv channels is a great deal narrower than the internal vestibule of BK channels (Li and Aldrich, 2004; Brelidze and Magleby, 2005; Ghatta et al., 2006; Geng et al., 2011; Zhou et al., 2011). Moreover, closed channels are blocked by both the Shaker "ball" peptide and large quaternary ammonium ions, indicating that the bundle crossing does not impede the passage of ions (Wilkens and Aldrich, 2006; Thompson and Begenisich, 2012). Although the evidence suggests that the BK activation gate is not intracellular as in Kv channels but may be located in the selectivity filter, there is evidence that certain key residues in the S6 transmembrane segment can play an important role in channel gating (Wang and Brenner, 2006; Wu et al., 2009; Chen and Aldrich, 2011; Zhou et al., 2011; Chen et al., 2014). Interestingly, some of the single point mutations introduced in S6 (e.g., L312Q and L312D, A313D, and A316D) produced permanently open channels at a wide range of voltages (Chen et al., 2014). Although it is reasonable to think that many amino acids could be involved in coupling, the results of other groups make us to believe that some residues are more important than others in determining BK channel gating. For example, Zhou et al. (2011) performed a cysteine scan throughout the murine BK S6 for each of the 28 amino acid residues. Consistent with our assumption that not all of the residues in S6 play the same role in gating, three residues, L312, F315, and P320, corresponding to L377, F380, and P385 in the human BK produced extremely shifted $G(V)$ curves. In these cases Zhou et al. (2011) were forced to assume the half-activation voltages and the voltage dependence of the $G(V)$ curves to perform an analysis of the periodicity of gating perturbations produced by cysteine mutations in the S6.

The use of mutagenesis, together with gating and macroscopic currents and MD simulations, allowed us in the present study to gain insight on the way that the S6 transmembrane segment participates as an integration node in the BK channel. Our results indicate that there are some key amino acid residues in the S6 that are central players in the coupling of electrical and calcium-binding energies with the pore opening. We have found an amino acid residue (F380) located in the S6 transmembrane segment that, once mutated to a small hydrophobic amino acid (alanine), profoundly modifies ion conduction without affecting the gating charge of the channel. Gating currents in the F380A mutant are found to be similar in their kinetic and steady properties to the WT BK channel. Moreover, the mutant channel allows the detection of gating currents in the presence of physiological K^+ concentrations, a result which shows that the voltage sensor can undergo its normal gating transitions in the presence or in the absence of permeant ions. Furthermore, the fact that ionic currents

can be detected when the internal Ca^{2+} concentration is high is a clear indication that this mutant channel can open upon membrane depolarization and is Ca^{2+} activated. In contrast, by using the allosteric HA model (Horrigan and Aldrich, 2002), it is possible to arrive at the conclusion that the F380A mutation uncouples voltage-dependent gating and calcium binding from voltage sensors and increases the energy difference between closed and open conformations of the channel by ~18.7 kJ/mol.

The present results show that replacing the large and hydrophobic phenylalanine by the small and hydrophobic alanine stabilizes the closed conformation of the BK channel. These results are at odds with what was proposed by Wu et al. (2009), because it is expected that a disruption of the interaction between F380 and L377, which interact only in the closed state, would stabilize the open state. A more plausible possibility is that actually residues F380 and L377 interact in both the closed and open state and the proper interaction is required for the normal gating. In fact, it is interesting to note that the interaction between the corresponding residue pair in KcsA (I100-F103) is present in both states, closed and open, as has been observed in the crystal structures of the closed (Doyle et al., 1998), the open, and the open inactivated (Cuello et al., 2010) structures, but only the former was used by Wu et al. (2009) for their MD simulations. We built a new open BK pore 3-D model based on MthK open structure (Posson et al., 2013), which has a larger radius at the mutation position than the KcsA-based model reported by Wu et al. (2009). The side chains of Phe380 and Leu377 in the BK model are not confronted to the pore and form a stable hydrophobic ring (Fig. 7 C). The nonbonded interaction energy between residue 380 and L377 is decreased by 20 kJ/mol when F380 is replaced by alanine. We hypothesize that the main stabilizing factor of the interaction between F380 and L377 of a neighboring subunit is the van der Waals interaction linking these two amino acids. Replacement of F380 by smaller hydrophobic amino acid residues should have the effect of stabilizing the closed state; note that this mutation produces a deactivation rate only five times faster than WT BK channel, whereas changes in L_0 are ~1,700 times; this implies that the effect is mainly on the activation rate, which becomes

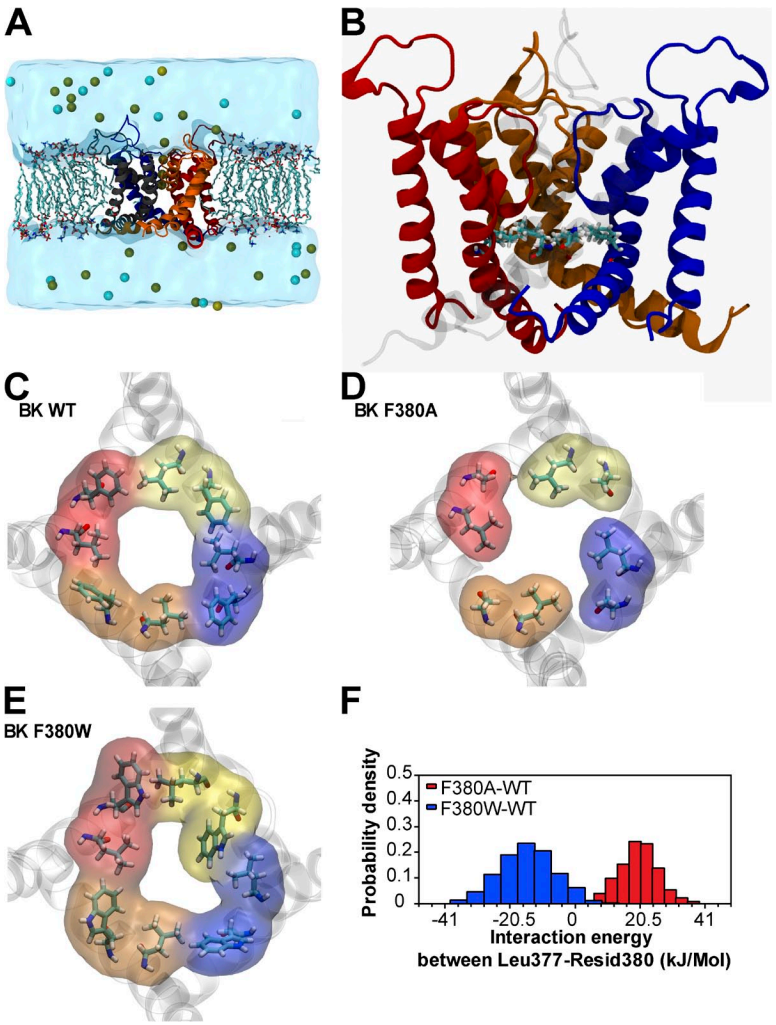

Figure 7. Molecular BK model and MD analysis. (A) Model built for open BK WT channel pore region (green balls are K^+ and blue balls are Cl^-). (B) Side view of the hydrophobic ring formed by the F380 and L377 residues in BK WT (one subunit is transparent to better view). (C–E) Top view of the hydrophobic ring formed by the 380 and 377 residues in BK WT, F380A, and F380W, respectively. (F) Interaction energy between L377 and 380 residues (WT is considered a reference).

340 times slower in the F380A mutant. In contrast, large hydrophobic amino acids such as tyrosine or tryptophan should strengthen the interaction between the L377 and 380 residue, increasing the intrinsic equilibrium constant L_0. As predicted, this mutation decreased the free energy difference between open and closed state, whereas the result of the in silico calculation of the energy between W380 and L377 was −16.5 kcal/mol when the F380 and L377 interaction energy is taken as reference (Fig. 7 F). Although it appears to be a clear negative correlation between the strength of the interaction and the free energy difference between open and closes states, the effects on the allosteric constants are not so clear and suggest that the hydrophobic ring is involved in the coupling between sensors and pore opening in a complex way. The coupling between voltage sensor and opening is decrease in both mutants, whereas E and C are decreased only in one of the mutants (F380A and F380W, respectively).

In the lack of a crystal structure of BK channel, we can only speculate about the possible interaction between the sensors and the structure formed by residues L377 and F380. Previous modeling (Carvacho et al., 2008) and the present molecular model (Fig. 7) show that the smallest diameter of the internal vestibule is attained at the level of F380. We hypothesized that the hydrophobic ring can be the fulcrum of a lever where the forces produced by the sensors converge. For example, the distances between the four S6 helixes can increase or decrease in response to calcium binding, and these movements could produce a stretching or relaxing of the structure formed by the set of the four S6 helixes, whereas this structure is really pivoting at the level of the hydrophobic ring and the diameter to this lever does not change substantially. In the case of voltage sensor, if the S4–S5 linker plays a similar role in BK channels as it does in Kv channels where this linker interacts with the S6, it is possible that the hydrophobic ring plays the same role as it does when the channel is activated by Ca^{2+}.

The gating phenotype of the F380A in the high Ca^{2+} mutant resembles that of the Shaker ILT mutant (Ledwell and Aldrich, 1999), where the voltage activation curve is shifted to the right along the voltage axis, whereas most of the gating charge moves at voltages at which channels are closed. In the ILT Shaker mutant, channel opening is associated with the charge movement linked to the last rate-limiting transition in the ILT activation pathway. Thus, the F380A mutant isolated the BK opening voltage-dependent transition from earlier gating transitions and may provide a valuable experiment tool for teasing out the molecular basis of structural transitions in the activation pathway of BK channels.

Additionally, our results also support the idea that the inner vestibule in BK channels plays an important role in determining unitary conductance (Lippiat et al., 2000). Our fluctuation analysis experiments show that the F380A and F380W mutations decrease the channel conductance by ∼60% and 50%, respectively.

We would like to thank Ms. Valeria Marquez and Ingrid Carvacho, who started the first theoretical and experimental approaches that led to our present understanding of the importance of residue F380 and Luisa Soto for excellent technical assistance.

This work was supported by FONDECYT grants 1110430 (to R. Latorre), 1120802 (to C. González), and 1131003 (to F. González-Nilo), ANILLO grant ACT1104 (to C. González) and grant RI-130006 (to R. Latorre and C. González). The Centro Interdisciplinario de Neurociencia de Valparaíso is a Millennium Institute supported by the Millenium Initiative of the Ministerio de Economía, Fomento y Turismo of Chile.

The authors declare no competing financial interests.

Lawrence G. Palmer served as editor.

Submitted: 6 March 2014
Accepted: 8 December 2014

REFERENCES

Alvarez, O., C. Gonzalez, and R. Latorre. 2002. Counting channels: a tutorial guide on ion channel fluctuation analysis. *Adv. Physiol. Educ.* 26:327–341.

Armstrong, C.M., and F. Bezanilla. 1974. Charge movement associated with the opening and closing of the activation gates of the Na channels. *J. Gen. Physiol.* 63:533–552. http://dx.doi.org/10.1085/jgp.63.5.533

Bao, L., and D.H. Cox. 2005. Gating and ionic currents reveal how the BK_{Ca} channel's Ca^{2+} sensitivity is enhanced by its β1 subunit. *J. Gen. Physiol.* 126:393–412. http://dx.doi.org/10.1085/jgp.200509346

Brayden, J.E., and M.T. Nelson. 1992. Regulation of arterial tone by activation of calcium-dependent potassium channels. *Science.* 256:532–535. http://dx.doi.org/10.1126/science.1373909

Brelidze, T.I., and K.L. Magleby. 2005. Probing the geometry of the inner vestibule of BK channels with sugars. *J. Gen. Physiol.* 126:105–121. http://dx.doi.org/10.1085/jgp.200509286

Brelidze, T.I., X. Niu, and K.L. Magleby. 2003. A ring of eight conserved negatively charged amino acids doubles the conductance of BK channels and prevents inward rectification. *Proc. Natl. Acad. Sci. USA.* 100:9017–9022. http://dx.doi.org/10.1073/pnas.1532257100

Candia, S., M.L. Garcia, and R. Latorre. 1992. Mode of action of iberiotoxin, a potent blocker of the large conductance Ca^{2+}-activated K^+ channel. *Biophys. J.* 63:583–590. http://dx.doi.org/10.1016/S0006-3495(92)81630-2

Carvacho, I., W. Gonzalez, Y.P. Torres, S. Brauchi, O. Alvarez, F.D. Gonzalez-Nilo, and R. Latorre. 2008. Intrinsic electrostatic potential in the BK channel pore: role in determining single channel conductance and block. *J. Gen. Physiol.* 131:147–161. http://dx.doi.org/10.1085/jgp.200709862

Chen, X., and R.W. Aldrich. 2011. Charge substitution for a deep-pore residue reveals structural dynamics during BK channel gating. *J. Gen. Physiol.* 138:137–154. http://dx.doi.org/10.1085/jgp.201110632

Chen, X., J. Yan, and R.W. Aldrich. 2014. BK channel opening involves side-chain reorientation of multiple deep-pore residues. *Proc. Natl. Acad. Sci. USA.* 111:E79–E88. http://dx.doi.org/10.1073/pnas.1321697111

Contreras, G.F., A. Neely, O. Alvarez, C. Gonzalez, and R. Latorre. 2012. Modulation of BK channel voltage gating by different auxiliary β subunits. *Proc. Natl. Acad. Sci. USA.* 109:18991–18996. http://dx.doi.org/10.1073/pnas.1216953109

Cox, D.H., J. Cui, and R.W. Aldrich. 1997. Allosteric gating of a large conductance Ca-activated K^+ channel. *J. Gen. Physiol.* 110:257–281. http://dx.doi.org/10.1085/jgp.110.3.257

Cuello, L.G., V. Jogini, D.M. Cortes, and E. Perozo. 2010. Structural mechanism of C-type inactivation in K^+ channels. *Nature.* 466:203–208. http://dx.doi.org/10.1038/nature09153

Doyle, D.A., J. Morais Cabral, R.A. Pfuetzner, A. Kuo, J.M. Gulbis, S.L. Cohen, B.T. Chait, and R. MacKinnon. 1998. The structure of the potassium channel: molecular basis of K^+ conduction and selectivity. *Science.* 280:69–77. http://dx.doi.org/10.1126/science.280.5360.69

Edgerton, J.R., and P.H. Reinhart. 2003. Distinct contributions of small and large conductance Ca^{2+}-activated K^+ channels to rat Purkinje neuron function. *J. Physiol.* 548:53–69. http://dx.doi.org/10.1113/jphysiol.2002.027854

Galvez, A., G. Gimenez-Gallego, J.P. Reuben, L. Roy-Contancin, P. Feigenbaum, G.J. Kaczorowski, and M.L. García. 1990. Purification and characterization of a unique, potent, peptidyl probe for the high conductance calcium-activated potassium channel from venom of the scorpion *Buthus tamulus*. *J. Biol. Chem.* 265:11083–11090.

Geng, Y., X. Niu, and K.L. Magleby. 2011. Low resistance, large dimension entrance to the inner cavity of BK channels determined by changing side-chain volume. *J. Gen. Physiol.* 137:533–548. http://dx.doi.org/10.1085/jgp.201110616

Gessner, G., K. Schönherr, M. Soom, A. Hansel, M. Asim, A. Baniahmad, C. Derst, T. Hoshi, and S.H. Heinemann. 2005. BK_{Ca} channels activating at resting potential without calcium in LNCaP prostate cancer cells. *J. Membr. Biol.* 208:229–240. http://dx.doi.org/10.1007/s00232-005-0830-z

Ghatta, S., D. Nimmagadda, X. Xu, and S.T. O'Rourke. 2006. Large-conductance, calcium-activated potassium channels: structural and functional implications. *Pharmacol. Ther.* 110:103–116. http://dx.doi.org/10.1016/j.pharmthera.2005.10.007

Giangiacomo, K.M., M.L. García, and O.B. McManus. 1992. Mechanism of iberiotoxin block of the large-conductance calcium-activated potassium channel from bovine aortic smooth muscle. *Biochemistry.* 31:6719–6727. http://dx.doi.org/10.1021/bi00144a011

Gola, M., and M. Crest. 1993. Colocalization of active KCa channels and Ca^{2+} channels within Ca^{2+} domains in helix neurons. *Neuron.* 10:689–699. http://dx.doi.org/10.1016/0896-6273(93)90170-V

Horrigan, F.T., and R.W. Aldrich. 1999. Allosteric voltage gating of potassium channels II. Mslo channel gating charge movement in the absence of Ca^{2+}. *J. Gen. Physiol.* 114:305–336. http://dx.doi.org/10.1085/jgp.114.2.305

Horrigan, F.T., and R.W. Aldrich. 2002. Coupling between voltage sensor activation, Ca^{2+} binding and channel opening in large conductance (BK) potassium channels. *J. Gen. Physiol.* 120:267–305. http://dx.doi.org/10.1085/jgp.20028605

Humphrey, W., A. Dalke, and K. Schulten. 1996. VMD: visual molecular dynamics. *J. Mol. Graph.* 14:33–38: 27–28. http://dx.doi.org/10.1016/0263-7855(96)00018-5

Kaczorowski, G.J., and M.L. García. 1999. Pharmacology of voltage-gated and calcium-activated potassium channels. *Curr. Opin. Chem. Biol.* 3:448–458. http://dx.doi.org/10.1016/S1367-5931(99)80066-0

Klauda, J.B., R.M. Venable, J.A. Freites, J.W. O'Connor, D.J. Tobias, C. Mondragon-Ramirez, I. Vorobyov, A.D. MacKerell Jr., and R.W. Pastor. 2010. Update of the CHARMM all-atom additive force field for lipids: validation on six lipid types. *J. Phys. Chem. B.* 114:7830–7843. http://dx.doi.org/10.1021/jp101759q

Lancaster, B., and R.A. Nicoll. 1987. Properties of two calcium-activated hyperpolarizations in rat hippocampal neurones. *J. Physiol.* 389:187–203.

Latorre, R., C. Vergara, and C. Hidalgo. 1982. Reconstitution in planar lipid bilayers of a Ca^{2+}-dependent K^+ channel from transverse tubule membranes isolated from rabbit skeletal muscle. *Proc. Natl. Acad. Sci. USA.* 79:805–809. http://dx.doi.org/10.1073/pnas.79.3.805

Ledwell, J.L., and R.W. Aldrich. 1999. Mutations in the S4 region isolate the final voltage-dependent cooperative step in potassium channel activation. *J. Gen. Physiol.* 113:389–414. http://dx.doi.org/10.1085/jgp.113.3.389

Li, W., and R.W. Aldrich. 2004. Unique inner pore properties of BK channels revealed by quaternary ammonium block. *J. Gen. Physiol.* 124:43–57. http://dx.doi.org/10.1085/jgp.200409067

Lippiat, J.D., N.B. Standen, and N.W. Davies. 2000. A residue in the intracellular vestibule of the pore is critical for gating and permeation in Ca^{2+}-activated K^+ (BK_{Ca}) channels. *J. Physiol.* 529:131–138. http://dx.doi.org/10.1111/j.1469-7793.2000.00131.x

Liu, Y., M. Holmgren, M.E. Jurman, and G. Yellen. 1997. Gated access to the pore of a voltage-dependent K^+ channel. *Neuron.* 19:175–184. http://dx.doi.org/10.1016/S0896-6273(00)80357-8

Marty, A. 1981. Ca-dependent K channels with large unitary conductance in chromaffin cell membranes. *Nature.* 291:497–500. http://dx.doi.org/10.1038/291497a0

Melo, F., and E. Feytmans. 1998. Assessing protein structures with a non-local atomic interaction energy. *J. Mol. Biol.* 277:1141–1152. http://dx.doi.org/10.1006/jmbi.1998.1665

Miranda-Rottmann, S., A.S. Kozlov, and A.J. Hudspeth. 2010. Highly specific alternative splicing of transcripts encoding BK channels in the chicken's cochlea is a minor determinant of the tonotopic gradient. *Mol. Cell. Biol.* 30:3646–3660. http://dx.doi.org/10.1128/MCB.00073-10

Moscoso, C., A. Vergara-Jaque, V. Márquez-Miranda, R.V. Sepúlveda, I. Valencia, I. Díaz-Franulic, F. González-Nilo, and D. Naranjo. 2012. K^+ conduction and Mg^{2+} blockade in a shaker Kv-channel single point mutant with an unusually high conductance. *Biophys. J.* 103:1198–1207. http://dx.doi.org/10.1016/j.bpj.2012.08.015

Orio, P., and R. Latorre. 2005. Differential effects of β1 and β2 subunits on BK channel activity. *J. Gen. Physiol.* 125:395–411. http://dx.doi.org/10.1085/jgp.200409236

Orio, P., P. Rojas, G. Ferreira, and R. Latorre. 2002. New disguises for an old channel: MaxiK channel beta-subunits. *News Physiol. Sci.* 17:156–161.

Pallotta, B.S., K.L. Magleby, and J.N. Barrett. 1981. Single channel recordings of Ca^{2+}-activated K^+ currents in rat muscle cell culture. *Nature.* 293:471–474. http://dx.doi.org/10.1038/293471a0

Patel, S., A.D. Mackerell Jr., and C.L. Brooks III. 2004. CHARMM fluctuating charge force field for proteins: II protein/solvent properties from molecular dynamics simulations using a nonadditive electrostatic model. *J. Comput. Chem.* 25:1504–1514. http://dx.doi.org/10.1002/jcc.20077

Phillips, J.C., R. Braun, W. Wang, J. Gumbart, E. Tajkhorshid, E. Villa, C. Chipot, R.D. Skeel, L. Kalé, and K. Schulten. 2005. Scalable molecular dynamics with NAMD. *J. Comput. Chem.* 26:1781–1802. http://dx.doi.org/10.1002/jcc.20289

Piskorowski, R.A., and R.W. Aldrich. 2006. Relationship between pore occupancy and gating in BK potassium channels. *J. Gen. Physiol.* 127:557–576. http://dx.doi.org/10.1085/jgp.200509482

Posson, D.J., J.G. McCoy, and C.M. Nimigean. 2013. The voltage-dependent gate in MthK potassium channels is located at the selectivity filter. *Nat. Struct. Mol. Biol.* 20:159–166. http://dx.doi.org/10.1038/nsmb.2473

Sali, A., and T.L. Blundell. 1994. Comparative protein modelling by satisfaction of spatial restraints. *In* Protein Structure by Distance Analysis. H. Bohr, and S. Brunak, editors. IOS Press, Amsterdam, Netherlands. 64–86.

Sigworth, F.J. 1980. The variance of sodium current fluctuations at the node of Ranvier. *J. Physiol.* 307:97–129.

Thompson, J., and T. Begenisich. 2012. Selectivity filter gating in large-conductance Ca^{2+}-activated K^+ channels. *J. Gen. Physiol.* 139: 235–244. http://dx.doi.org/10.1085/jgp.201110748

Toro, L., M. Wallner, P. Meera, and Y. Tanaka. 1998. Maxi-K(Ca), a unique member of the voltage-gated K channel superfamily. *News Physiol. Sci.* 13:112–117.

Wang, B., and R. Brenner. 2006. An S6 mutation in BK channels reveals β1 subunit effects on intrinsic and voltage-dependent gating. *J. Gen. Physiol.* 128:731–744. http://dx.doi.org/10.1085/jgp.200609596

Wells, D.B., S. Bhattacharya, R. Carr, C. Maffeo, A. Ho, J. Comer, and A. Aksimentiev. 2012. Optimization of the molecular dynamics method for simulations of DNA and ion transport through biological nanopores. *Methods Mol. Biol.* 870:165–186. http://dx.doi.org/10.1007/978-1-61779-773-6_10

Wilkens, C.M., and R.W. Aldrich. 2006. State-independent block of BK channels by an intracellular quaternary ammonium. *J. Gen. Physiol.* 128:347–364. http://dx.doi.org/10.1085/jgp.200609579

Wu, Y., Y. Xiong, S. Wang, H. Yi, H. Li, N. Pan, F.T. Horrigan, Y. Wu, and J. Ding. 2009. Intersubunit coupling in the pore of BK channels. *J. Biol. Chem.* 284:23353–23363. http://dx.doi.org/10.1074/jbc.M109.027789

Yan, J., and R.W. Aldrich. 2012. BK potassium channel modulation by leucine-rich repeat-containing proteins. *Proc. Natl. Acad. Sci. USA.* 109:7917–7922. http://dx.doi.org/10.1073/pnas.1205435109

Yu, F.H., and W.A. Catterall. 2004. The VGL-chanome: a protein superfamily specialized for electrical signaling and ionic homeostasis. *Sci. STKE.* 2004:re15.

Zhou, Y., X.M. Xia, and C.J. Lingle. 2011. Cysteine scanning and modification reveal major differences between BK channels and Kv channels in the inner pore region. *Proc. Natl. Acad. Sci. USA.* 108:12161–12166. http://dx.doi.org/10.1073/pnas.1104150108